



Article

Integrated Assessments of Land Degradation in the Three-Rivers Headwater Region of China from 2000 to 2020

Yao Pan ^{1,2}, Yunhe Yin ^{1,*}  and Wei Cao ¹

¹ Key Laboratory of Land Surface Pattern and Simulation, Institute of Geographic Sciences and Natural Resources Research, Chinese Academy of Sciences, Beijing 100101, China; pany.17s@igsnr.ac.cn (Y.P.)

² University of Chinese Academy of Sciences, Beijing 100049, China

* Correspondence: yinyh@igsnr.ac.cn

Abstract: Since the 1970s, certain areas within the Three-Rivers Headwater Region (TRHR) of China have faced severe land degradation due to the combined effects of climate change and human activities, leading to restricted ecological service functions and hindering the achievement of sustainable development goals (SDGs). Land degradation in the TRHR has received widespread attention. However, the current research mainly focuses on single-dimensional degradation and lacks a comprehensive evaluation of patterns and structures, as well as above-ground and underground assessments. To address this gap, this study employed the SDG indicator 15.3.1 framework, comprehensively considering fragmentation and habitat quality index based on land cover changes, grassland degradation index, and soil water erosion index. These indexes represent the three land degradation pathways of landscape degradation, vegetation degradation, and soil erosion. This study assessed land degradation patterns in the TRHR from 2000 to 2020. Results show that approximately 44.67% of the TRHR experienced land degradation during this period, mainly in meadow-dominated regions. Additionally, 5.64% of the regions experienced the superimposition of two or more land degradation pathways, with the frequent coexistence of soil erosion and grassland degradation, accounting for 4.1% of the affected areas. Landscape degradation affected approximately 2.39% of the regions, characterized by increased grassland fragmentation or habitat quality degradation. In terms of grassland degradation, 22.26% of the regions showed medium degradation, while 7.21% and 5.63% experienced moderate and severe degradation, respectively. Moreover, approximately 13.36% of the region faced a worsening situation of soil erosion. Approximately 55.34% of the study area underwent land improvement, with significant enhancements mainly concentrated in the western and eastern regions. The regrowth of grassland in the western region and the enhancement and homogenization of grassland productivity in the eastern region played pivotal roles in promoting land improvement. This study provides critical insights into the land degradation pattern in the TRHR over the past 20 years, offering valuable references for formulating and implementing measures to protect and construct the ecological security barrier of the plateau.

Keywords: landscape pattern; grassland degradation; soil erosion; land degradation; Three-Rivers Headwater Region



Citation: Pan, Y.; Yin, Y.; Cao, W. Integrated Assessments of Land Degradation in the Three-Rivers Headwater Region of China from 2000 to 2020. *Remote Sens.* **2023**, *15*, 4521. <https://doi.org/10.3390/rs15184521>

Academic Editor: Elias Symeonakis

Received: 24 July 2023

Revised: 7 September 2023

Accepted: 12 September 2023

Published: 14 September 2023



Copyright: © 2023 by the authors. Licensee MDPI, Basel, Switzerland. This article is an open access article distributed under the terms and conditions of the Creative Commons Attribution (CC BY) license (<https://creativecommons.org/licenses/by/4.0/>).

1. Introduction

Land is the fundamental resource for human survival, providing us with food and materials while also playing a crucial role in regulating and supporting ecosystem services [1]. However, land degradation has become a global issue due to climate change and human activities [2]. Global assessments indicate that between 1 and 6 billion hectares of land are currently experiencing degradation [3]. Additionally, the increasing frequency of extreme events and human overexploitation of natural resources further exacerbate localized land degradation trends [4,5]. In this context, the Tibetan Plateau, as a critical component of the cryosphere, faces an extremely fragile environment [6]. Climate warming has

accelerated processes of land degradation, such as permafrost thawing, leading to severe consequences, such as soil nutrient loss, reduction in ecosystem services, and the release of large amounts of carbon stored in permafrost [7,8]. Therefore, determining and monitoring specific degradation thresholds and precisely identifying the location, extent, and status of land degradation in the region are crucial to achieve land degradation neutrality.

The Three-Rivers Headwater Region (TRHR), located in the hinterland of the Tibetan Plateau, plays a crucial role in various ecosystem services, such as water conservation and regulation, making it a vital component of the national ecological security barrier [9]. However, the alpine vegetation coverage in this area is relatively sparse, rendering its ecosystem fragile and highly susceptible to human disturbances and climate change impacts [10]. Since the 1970s, certain areas of the TRHR have encountered numerous land degradation issues, including grassland desertification, wetland loss, permafrost thawing, and soil erosion [11–14]. These land degradation issues limit the ecological service functions of the TRHR, thus posing constraints on the achievement of sustainable development goals (SDGs) [15]. The combined effects of livestock grazing and climate change pose substantially high risks of degradation in this area [16]. In recent years, the application of remote sensing technology has promoted land degradation assessments over large areas [17]. Scholars have conducted assessments of specific aspects including landscape patterns [18,19], soil erosion [20], grassland degradation [21], and black soil beaches [22]. While some comprehensive assessments of salinization, desertification, and soil erosion have been carried out [15], these studies have not fully captured the comprehensive changes in land cover, vegetation, and soil parameters. Additionally, the use of cross-sectional assessment methods fails to capture the long-term trends of land degradation. Therefore, it remains crucial to comprehensively monitor the current status of land degradation in the TRHR for effective and sustainable ecosystem management.

The United Nations Convention to Combat Desertification (UNCCD) utilized the three sub-indicators of sustainable development goal (SDG) indicator 15.3.1 to evaluate land degradation, including land cover (indicator: land cover type), land productivity (indicator: net primary productivity, NPP), and carbon stock (indicator: soil organic carbon, SOC), which are widely accepted for monitoring global land degradation [4,23]. However, selecting suitable indicators to assess local land degradation when applied to specific regions is crucial due to the spatial heterogeneity of land degradation and data limitations [5,24]. Considering that solely using the actual land cover degradation area might overlook its impact on the surrounding land, this study utilizes the fragmentation and habitat quality index based on land use change to comprehensively evaluate the degradation of landscape structure and quality in the TRHR [25]. Land productivity sub-indicators are based on the concept that the loss of vegetation yield in productive land may lead to land degradation and vice versa [26]. Due to challenges in accurately estimating net primary productivity (NPP) from remote sensing data, vegetation indexes (such as the normalized difference vegetation index (NDVI)) are often used as substitutes for NPP, as they exhibit a high correlation and indication ability with NPP [27]. The SOC indicator is often underrepresented in many regions due to difficulties in accessing sufficient large-scale SOC data [28]. As an alternative to SOC, soil erosion assessment indexes provide a successful representation of changes in land capacity [29].

To gain a more comprehensive understanding of land degradation in the TRHR, this study considers the unique characteristics of the alpine ecosystem in this area and employs various land degradation indicators for regional improvement and application. Specifically, based on the calculation framework of SDG 15.3.1, this study utilizes the fragmentation and habitat quality index based on land cover changes, the grassland degradation index, and the soil water erosion index to, respectively, characterize the three pathways of landscape degradation, vegetation degradation, and soil erosion. Additionally, this study emphasizes the analysis of indicator trends and states, evaluating land degradation in the TRHR from 2000 to 2020, rather than solely focusing on a single time snapshot. This provides a deeper understanding of the trend and evolution of land degradation in the

study area and lays a solid research foundation for the sustainable development of alpine ecosystems. The objectives of this study are as follows: (1) to quantify the spatial patterns of landscape degradation, vegetation degradation, and soil erosion intensification in the TRHR from 2000 to 2020 by combining the trends of sub-indicators and changes relative to the baseline period and (2) to comprehensively assess the spatial distribution of land improvement or degradation in the TRHR from 2000 to 2020, considering all three land degradation pathways.

2. Materials and Methods

2.1. Study Area

The TRHR ($31^{\circ}39'–36^{\circ}12'N$, $89^{\circ}45'–102^{\circ}23'E$, Figure 1) is located in the hinterland of the Tibetan Plateau, with a series of mountains with an altitude of more than 4000 m. The TRHR covers a total area of $36.63 \times 10^4 \text{ km}^2$ and includes 20 administrative counties in Guoluo, Yushu, Hainan and Huangnan Tibetan Autonomous Prefectures, and Tanggula Mountain Town in Geermu City (Figure 1).

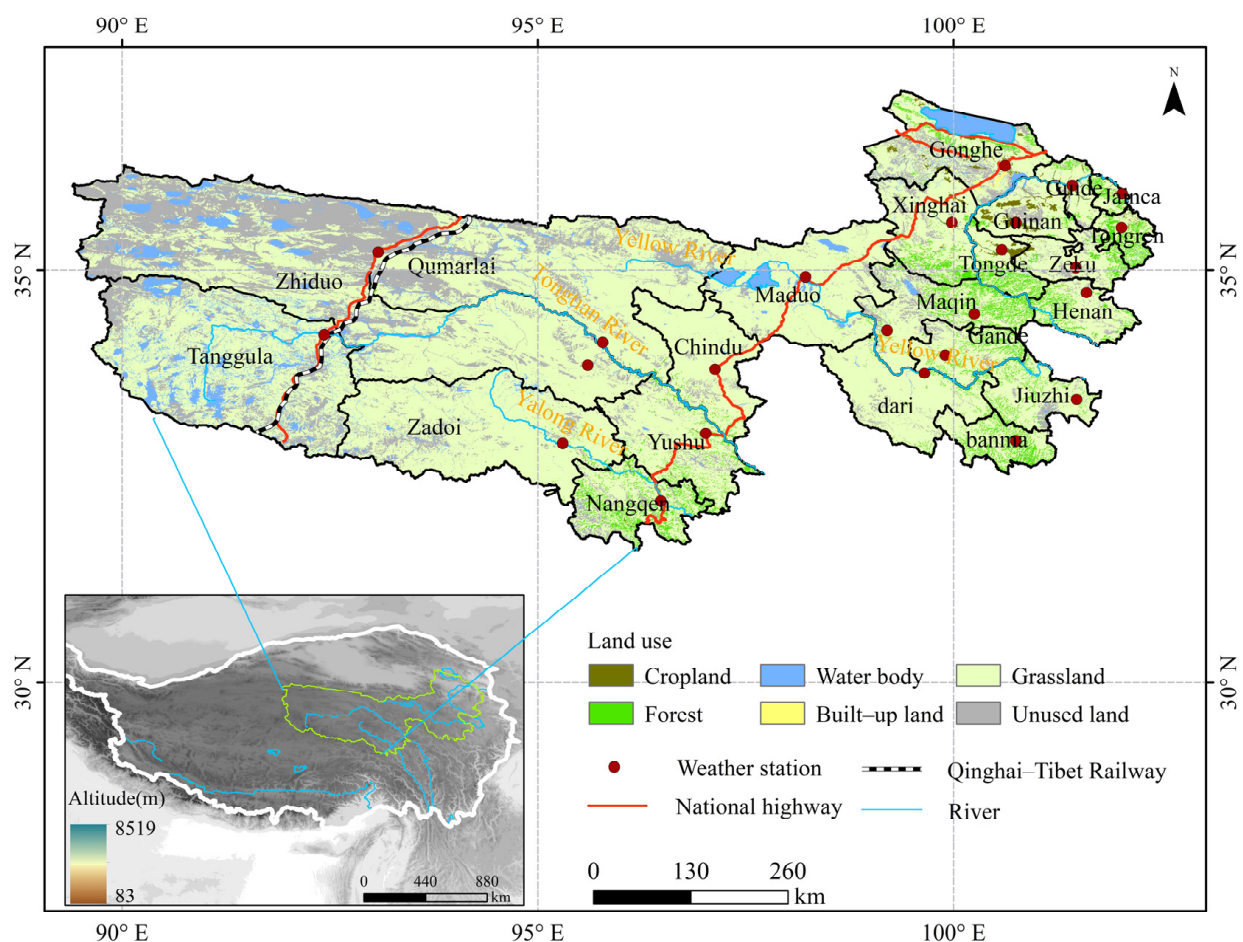


Figure 1. Location, land use, and grassland types in the Three-Rivers Headwater Region.

2.2. Data

Table 1 presents the descriptions and sources of various data used in this study. All raster data were standardized to a resolution of 500 m using ArcGIS 10.5.

Table 1. Basic information regarding the data sets used in this research.

Data Type	Data Use	Data Format	Data Source
Precipitation	Rainfall erodibility	Grid, 500 m resolution, from 2000 to 2020.	National Climate Center of the China Meteorological Administration (http://data.cma.cn/ , accessed on 1 September 2022). 500 m resolution grid is interpolated using the professional meteorological interpolation software ANUSPLINA-version 4.4 (http://fennerschool.anu.edu.au/files/anusplin44.pdf , accessed on 1 September 2022)
Land use	Fragmentation index, habitat quality, and soil erosion	Grid, 30 m resolution, 2000, 2005, 2010, 2015, and 2020	Resource and Environment Center of Chinese Academy of Sciences (http://www.resdc.cn , accessed on 1 September 2022)
Digital elevation model (DEM)	Soil erosion	Grid, 500 m resolution, 2020	Resource and Environment Center of Chinese Academy of Sciences (http://www.resdc.cn , accessed on 1 September 2022)
NDVI	Habitat quality, grassland degradation	Grid, 500 m resolution, 16-day scale from 2000 to 2020.	MOD13A1 (https://modis.gsfc.nasa.gov/data/ , accessed on 1 September 2022)
Road	Habitat quality, grassland degradation	Shapefile, 2000 and 2015	Geographic Data Platform, School of Urban and Environmental Sciences, Peking University (http://geodata.pku.edu.cn , accessed on 1 September 2022)
Eco-function zones of the TRHR	Habitat quality	Shapefile	The data are converted into vector format using the eco-function zones map of the Three-River-Source National Park of China.
Soil properties (The fraction of sand, silt, and clay. The content of soil organic carbon.)	Water conservation and soil erosion	Grid, 30 arc second, 1995	Harmonized world soil database (HWSD) v1.2 (http://www.fao.org/soils-portal/soil-survey/soil-maps-and-databases/harmonized-world-soil-database-v12/en/ , accessed on 1 September 2022)
Soil depth	Water conservation	Grid, 1 km resolution, 1990	Soil Data Center, National Earth System Science Data Sharing Infrastructure, National Science and Technology Infrastructure of China (http://soil.geodata.cn , accessed on 1 September 2022)

2.3. Methods

2.3.1. Land Degradation Intensity Classification and Overlay Analysis of Degradation Pathways

Land Degradation Intensity Classification

This study adhered to the calculation framework of SDG 15.3.1, utilizing the fragmentation and habitat quality indexes based on land use change, as well as the grassland degradation and water erosion indexes, to assess three land degradation pathways, which include landscape structure and quality degradation, vegetation degradation, and soil erosion (Table 2). SDG indicator 15.3.1 considers the loss of land cover types as the primary manifestation of land degradation [23]. Land use change affects the landscape pattern and habitat quality of ecosystems [30]. Specifically, land use changes can promote the formation of new edges or modify existing edges, resulting in landscape fragmentation and fundamentally affecting the structure and function of ecosystems [31]. The landscape fragmentation index can characterize not only the reduction in land cover area but also the degree of connectivity between remaining patches [32]. The decline in habitat quality based on land use reflects the loss of ecosystem service capacity provided by the landscape [33,34]. Therefore, the level of landscape degradation can be comprehensively reflected from the perspectives of structure and function by combining landscape fragmentation and habitat quality indexes. SDG indicator 15.3.1 recommends using the decreasing trend of NPP to measure vegetation degradation [23]. However, accurately estimating NPP through remote sensing data is more challenging than estimating NDVI [4]. NDVI has been applied in previous studies to assess vegetation degradation and has demonstrated a strong correlation with NPP [27]. In this study, we followed the approach of Li et al. [21] to assess grassland degradation in the study area using NDVI and considering its spatial heterogeneity in terms of status and trends. The third aspect of SDG indicator 15.3.1 focuses on the reduction in soil organic carbon (SOC). However, the SOC indicator is underrepresented in

most regions [28]. Significant uncertainties currently exist, and consistent time series data regarding the reliability and accuracy of SOC product data in plateau areas are lacking, increasing the difficulty of assessments through SOC [35]. As an alternative indicator to SOC, soil erosion assessment indicators can successfully represent changes in land capability [29]. The soil water erosion index was selected in this study to evaluate soil erosion in the TRHR [15].

Table 2. Division of land degradation intensity.

Degradation Pathways	Evaluation Index	Land Degradation Intensity ¹	Classification Method
Landscape degradation (structure and quality)	Fragmentation index	Apparent improvement	Compared with the images in 2000 and 2020, the relative percentage of the fragmentation index decreased by more than 20%
		Slight improvement	Compared with the two images, the relative percentage of the fragmentation index decreased by 10–20%
		Slight degradation	Compared with the two images, the relative percentage of the fragmentation index increased by 10–20%
		Moderate degradation	Compared with the two images, the relative percentage of the fragmentation index increased by 20–50%
		Severe degradation	Compared with the two images, the relative percentage of the fragmentation index increased by more than 50% or the grassland patches disappeared completely
	Habitat quality	Apparent improvement	The habitat quality demonstrated a positive trend, with the change period increasing by over 20% compared to the average value during the baseline period
		Slight improvement	The habitat quality demonstrated a positive trend, with the change period increasing by 10–20% compared to the average value during the baseline period
		Slight degradation	The habitat quality exhibited a declining trend, with the change period decreasing by 10–20% compared to the average value during the baseline period
		Medium degradation	The habitat quality exhibited a declining trend, with the change period decreasing by 20–50% compared to the average value during the baseline period
		Severe degradation	The habitat quality exhibited a declining trend, with the change period decreasing by over 50% compared to the average value during the baseline period
Vegetation degradation	Grassland degradation	Apparent improvement	NDVI increased and spatial heterogeneity decreased simultaneously
		Slight improvement	NDVI and spatial heterogeneity increased (regions with NDVI < 0.2)
		Slight degradation	NDVI and spatial heterogeneity increased (regions with NDVI > 0.2)
		Medium degradation	NDVI decreased and spatial heterogeneity increased
		Severe degradation	NDVI and spatial heterogeneity decreased simultaneously (regions with NDVI > 0.2)

Table 2. Cont.

Degradation Pathways	Evaluation Index	Land Degradation Intensity ¹	Classification Method
Soil erosion	Soil water erosion	Apparent improvement	The change rate of erosion modulus for multiple years is below $-0.5 \text{ t/hm}^2/\text{a}$
		Slight improvement	The change rate of erosion modulus for multiple years ranges between -0.5 and $-0.05 \text{ t/hm}^2/\text{a}$
		Slight degradation	The change rate of erosion modulus for multiple years ranges between 0.05 and $0.2 \text{ t/hm}^2/\text{a}$
		Medium degradation	The change rate of erosion modulus for multiple years ranges between 0.2 and $0.5 \text{ t/hm}^2/\text{a}$
		Severe degradation	The change rate of erosion modulus for multiple years is above $0.5 \text{ t/hm}^2/\text{a}$

¹ Values ranging from slight degradation to slight improvement can be classified as a stable state.

This research mainly focused on the fragmentation of alpine grasslands in the TRHR, a vital component covering over 70% of the area. The intensification of fragmentation and degradation of habitat quality was determined by comparing the change period (2011–2020) with the baseline period (2000–2010). The classification of habitat quality degradation also considered the changing trends over five time sections (every five years from 2000 to 2020). The work of Li et al. [21] (Section 2.3.3) was used as a reference when categorizing the intensity of grassland degradation. Furthermore, the threshold from Liu et al. [36] concerning the changing trend of the soil erosion modulus was integrated to assess the extent of soil erosion aggravation in the study area.

Overlay Analysis of Degradation Pathways

This study follows the principle of “One Out, All Out” in SDG 15.3, which means that if any sub-indicators in a land unit show degradation, then the land unit will be classified as degraded. However, this study proposes to further classify the intensity of land degradation by considering the trend and state change of sub-indicators. The trend refers to the rate of sub-indicator value changes in a land unit calculated using the least squares method from 2000 to 2020. The state refers to the change ratio of the change period (2011–2020) compared to the average value of the baseline period (2000–2010). The degradation degree of a land unit is determined on the basis of the most severe degradation state observed among all sub-indicators (slight < medium < severe). Conversely, the land improvement status is defined on the basis of the highest level of improvement observed among all sub-indicators (slight < apparent).

2.3.2. Landscape Structure and Quality Degradation

Fragmentation Index

The high fragmentation index of grassland patches indicates severe degradation of the grassland ecosystem. Moreover, as the patches become fragmented, the large original patches gradually break up into numerous small patches, leading to an increased proportion of patch edge area per unit area. The reticular fragmentation index (RFI) can be utilized as a measure to adequately describe the fragmentation level within the ecosystem [37]:

$$\text{RFI} = \frac{(\text{PSB} + \text{ED})}{2} \quad (1)$$

$$\text{ED} = \frac{\text{TE}}{\text{A}} \quad (2)$$

The RFI is expressed as a percentage (%). The RFI is calculated based on the basis of land use change statistics for a $500 \text{ m} \times 500 \text{ m}$ grid. This index considers the proportion

of non-grassland area (PSB), the perimeter (m) of each grassland patch (TE), the total area of grassland (A) in square meters (m²), and the proportion of edge area (ED). The TE is determined by measuring the grass edges observed within each 500 m × 500 m grid, as outlined by Fischer et al. [38].

Habitat Quality

This study assessed habitat quality at five-year intervals, specifically in 2000, 2005, 2010, 2015, and 2020. The calculation of habitat quality involved the integration of the mean value of NDVI during the growing season, along with the outcomes generated using the InVEST Habitat Quality model [39]:

$$Q_x = Q_i \times M_{NDVI} \quad (3)$$

where Q_i represents the habitat quality of grid x , which is evaluated using the InVEST habitat quality model, and M_{NDVI} represents the average NDVI of grid x during the growing season.

When calculating habitat quality using the InVEST model, the overall threat level to the habitat type is considered.

$$Q_i = H_t \left(1 - \left(\frac{D_{xt}^z}{D_{xt}^z + K^z} \right) \right) \quad (4)$$

where H_t is habitat suitability, and K corresponds to the half-saturation constant, typically assigned a value of 0.05. The parameter z represents a scale parameter that reflects spatial heterogeneity in the analysis. Additionally, D_{xj} represents the total threat level of grid cell x under a specific land type. The habitat quality output score generated using the InVEST model ranges from 0 to 1, with high scores indicating high habitat quality [40].

Rural settlements, croplands, main roads, and railways were selected as threat sources in this study. The Qinghai–Tibet Railway, which was completed and opened for traffic in July 2006, passes through the TRHR. Therefore, starting in 2005, this study considered the impact of the railway on the habitat quality in the TRHR. The influence distance and weight of threat factors, habitat suitability, and relative sensitivity to different threat sources were based on previous research [41–44], and the parameters were adjusted in accordance with the field survey data in the study area (Table 3). Additionally, the TRHR was divided into core protection, ecological conservation and restoration, and traditional utilization areas in 2016; the accessibility layer of threat sources was considered when calculating habitat quality in 2020, and the actual threats to the reserve were revised. As per the recommendations of the model manual, accessibility values of 0.2, 0.8, and 1 were set for the core protection area, ecological conservation and restoration area, and traditional utilization area, respectively.

Table 3. Threat factors and related coefficients and sensitivity of habitat types to each threat factor.

Threat		Rural Settlements	Cropland	Main Road	Railway	
Maximum influence distance		5	3	10	10	
Weight		0.2	0.2	0.3	0.3	
Distance–decay function		Index	Linear	Linear	Index	
Land Use	Habitat Type	Habitat Suitability				
Agriculture	Cropland	0.3	0.7	0	0.6	0.65
Forest	Forest	1	0.9	0.8	0.8	0.85
	Shrub forest	0.85	0.8	0.7	0.7	0.75
	Sparse woodland	0.9	0.9	0.8	0.8	0.85
	Other woodlands	0.8	0.9	0.8	0.8	0.85

Table 3. Cont.

	Threat		Rural Settlements	Cropland	Main Road	Railway
Grassland	Highly covered grassland	0.8	0.8	0.7	0.7	0.75
	Medium-covered grassland	0.75	0.8	0.7	0.7	0.75
	Low-coverage grassland	0.7	0.8	0.7	0.7	0.75
Waterbody	Rivers, lakes, reservoirs, and beaches	0.7	0.9	0.8	0.8	0.85
	Permanent glacier	0	0	0	0	0
	Tideland	0.1	0	0.3	0.3	0.35
Built-up area	Rural settlements	0	0	0	0	0
	Other construction land	0	0	0	0	0
Unutilized land	Sand, bare land, etc.	0.2	0.6	0.5	0.5	0.55

2.3.3. Grassland Degradation

Li et al. [21] classified the degree of grassland degradation into five states based on different vegetation change trends and variations in spatial heterogeneity. The first state signifies an increase in NDVI and a decrease in spatial heterogeneity, indicating enhanced productivity, homogeneity, and improved growth conditions of the grassland. This state is defined as “apparent improvement”. In the second state, areas with sparse or no vegetation ($NDVI < 0.2$) experience an increase in NDVI and spatial heterogeneity, indicating vegetation regeneration. This state is defined as “slight improvement”. The third state occurs in vegetation growth areas ($NDVI > 0.2$), where the increase in NDVI is attributed to invasive species, leading to increased vegetation greenness and subsequent spatial heterogeneity. This state is defined as “slight degradation”. The fourth state involves a decrease in NDVI and an increase in spatial heterogeneity, representing a “medium degradation” of the grassland. In areas with sparse vegetation and low vegetation coverage ($NDVI < 0.2$), when NDVI and spatial heterogeneity decrease simultaneously, it indicates a transition from a patchy stage to a bare land stage, defined as “severe degradation”.

In this study, the median NDVI for each month from May to September of a year was used as the annual NDVI value. A 3×3 moving window ($1500 \text{ m} \times 1500 \text{ m}$) was applied to calculate the coefficient of variation (CV) of the NDVI, excluding the influence of rivers and roads on the NDVI to reduce spatial heterogeneity. Refer to the research of Li et al. [21] for a detailed calculation process.

2.3.4. Soil Water Erosion

Based on the RUSLE model, the soil erosion intensity affected by rainfall in the TRHR is evaluated using the following calculation formula:

$$S = R \times K \times LS \times C \times P \quad (5)$$

where S represents the soil erosion modulus per unit area ($\text{t}/\text{hm}^2/\text{a}$), R stands for the rainfall erodibility factor ($\text{MJ}\cdot\text{mm}/(\text{t}\cdot\text{hm}^2\cdot\text{a})$), K is the soil erodibility factor ($\text{t}\cdot\text{h}/(\text{MJ}\cdot\text{mm})$), and LS represent the slope length factor and the slope gradient factor, respectively. C is the vegetation coverage and management factor (ranging between 0 and 1), and P is the soil erosion control practice factor (ranging between 0 and 1).

In this study, the R factor for each station in the TRHR is calculated every half month, and the elevation is used as a covariate to interpolation covariate for the entire region. The formula for calculating the R factor for half a month is as follows:

$$R = \alpha \sum_{j=1}^{15} D_j^\beta \quad (6)$$

$$\alpha = 21.586\beta^{-7.1891} \quad (7)$$

$$\beta = 0.8363 + \frac{18.144}{P_{d12}} + \frac{24.455}{P_{y12}} \quad (8)$$

where R represents the rainfall erosivity factor for a period of half a month. P_{d12} refers to the average daily precipitation over multiple years but only considers the dates with rainfall greater than 12 mm. By contrast, the precipitation on days with rainfall lower than 12 mm is considered 0. Finally, P_{y12} represents the multi-year average of the cumulative value of rainfall with daily rainfall greater than 12 mm. The R factors for half a month are accumulated in this study to obtain the R factors for the entire year.

The monthly NDVI value, obtained using the maximum synthesis method, was used to calculate the vegetation coverage and management factor, denoted as C. This factor represents the impact of vegetation growth on soil erosion:

$$C = \begin{cases} 1, & f = 0 \\ 0.6508 - 0.3436\lg(f), & 0 \leq f \leq 78.3 \\ 0, & f > 78.3 \end{cases} \quad (9)$$

The formula for calculating vegetation coverage (f) is as follows:

$$f = \frac{NDVI - NDVI_{soil}}{NDVI_{max} - NDVI_{soil}} \quad (10)$$

The variable $NDVI_{soil}$ represents the NDVI value of bare soil pixels, while $NDVI_{max}$ represents the value of pure vegetation pixels. In this study, the monthly NDVI data for the study area were used to approximate the sum of ideal states for vegetation coverage calculation. The maximum synthesis method was employed to obtain the monthly vegetation coverage values.

The gradient of the study area is generated using the slope tool provided by ArcGIS. This gradient is then further processed to obtain the gradient factor (S) for the study area:

$$S = \begin{cases} 10.8 \times \sin(\theta) + 0.03, & \theta < 9\% \\ 16.8 \times \sin(\theta) - 0.5, & 9\% \leq \theta \leq 18\% \\ 21.91 \times \sin(\theta) - 0.96, & \theta > 18\% \end{cases} \quad (11)$$

where θ is the slope.

$$L = \frac{\lambda}{22.13}^m \quad (12)$$

$$m = \frac{\gamma}{(1 + \gamma)} \quad (13)$$

$$\gamma = \frac{\sin(\theta)/0.0896}{3 * \sin(\theta)^{0.8} + 0.56} \quad (14)$$

where L represents the slope length (m) and the parameters γ and m are dimensionless constants according to the percent slope θ , where θ is the slope.

In this study, the soil erodibility factor was calculated using the EPIC model [45]:

$$K = \left\{ 0.2 + 0.3 \exp \left[-0.0256 SAN \left(1 - \frac{SIL}{100} \right) \right] \right\} \left(\frac{SIL}{CLA + SIL} \right)^{0.3} \\ \times \left(1 - \frac{0.25C}{C + \exp(3.72 - 2.95C)} \right) \\ \times \left(1 - \frac{0.7SNI}{SNI + \exp(-5.51 + 22.9SNI)} \right) \quad (15)$$

where SAN, CLA, and C are the sand content (%), clay content (%), and soil organic carbon content (%), respectively. The calculated K factor is multiplied by 0.1317 to facilitate conversion into international units (t·h/(MJ·mm)).

The P factor for soil and water conservation measures is defined as the ratio of soil loss after implementing conservation measures to soil loss without any measures. Previous research results were utilized in this study as a reference when assigning P factor values [11]. Specifically, cropland, forest, other woodland, grassland, built-up land, and unused land were assigned P factor values of 0.4, 1, 0.7, 1, 0, and 1, respectively.

Soil erosion is commonly categorized into six different grades based on its intensity (Table 4) according to the Standards of SL 190–2007 for the Classification and Gradation of Soil Erosion promulgated by the Ministry of Water Resources (China).

Table 4. The gradation and classification of soil water erosion intensity.

Classification	Water Erosion Intensity (t/hm ² /a)
micro	<10
mild	10–25
moderate	25–50
strong	50–80
extreme	80–150
severe	>150

2.3.5. Total Research Approach

In this study, the first step involves determining the multi-year status of degradation indicators (RFI, habitat quality, grassland degradation index, and soil water erosion). This step is followed by assessing the land degradation intensity via analysis of the trends and state changes over multiple years. Landscape degradation is assessed by combining changes in landscape structure and quality. Finally, the land degradation pattern in the TRHR from 2000 to 2020 is obtained (Figure 2) by overlaying landscape degradation, vegetation degradation, and soil erosion in the land degradation pathways.

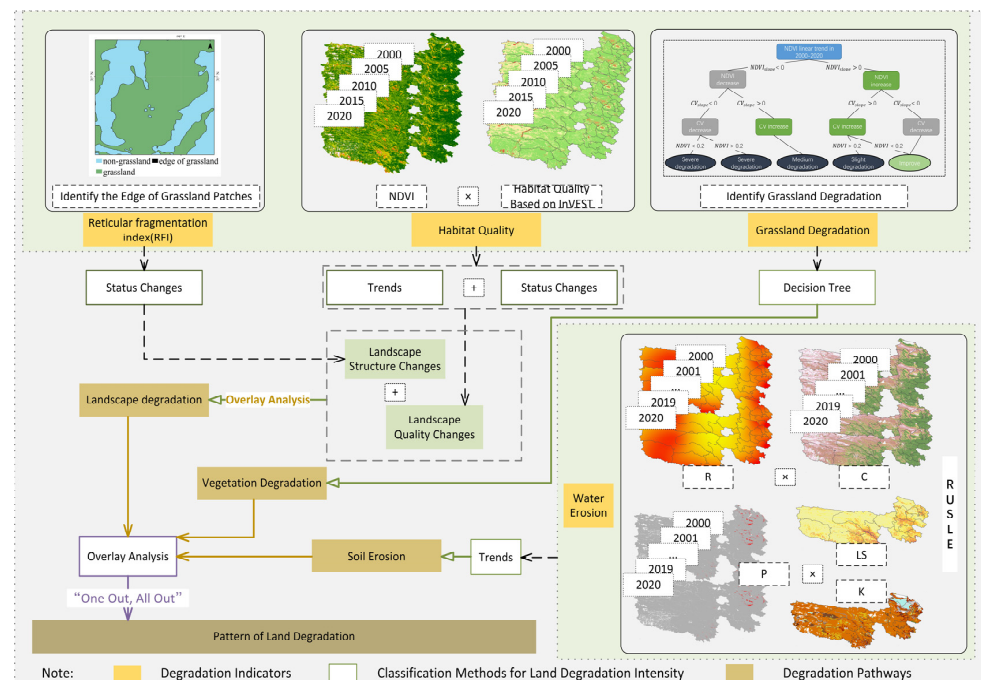


Figure 2. Implementation flow chart of this study.

3. Results

3.1. Superimposition of Three Degradation Pathways

Three main degradation pathways were overlapped to analyze the multidimensional existence of land degradation pathways: landscape (L) degradation, vegetation (V) degra-

gradation, and soil erosion (S) intensification. Their spatial distribution patterns in the TRHR were also analyzed. The analysis results revealed that land improvement from 2000 to 2020 was the main trend in the TRHR, with the improvement areas mainly distributed in the western and northeastern parts of the study area (Figure 3c). Notably, apparent land improvement was observed in Zhiduo County, Tanggula Mountain Town, Maduo County, Dari County, and Zeku County (as indicated in Figure 3b). Simultaneous improvement in “EV” was mainly observed in the western and southeastern parts of the study area. Simultaneous improvement in “LV” mainly occurred in the northern part of the study area. The area with simultaneous improvement in all three aspects (LEV) was relatively small, accounting for only 1.79% of the total area (Table 5). The regrowth of grassland in the western region and the improvement and homogenization of grassland productivity in the eastern region played pivotal roles in promoting land improvement in the TRHR.

Table 5. Proportion of land degradation types and intensity (%).

Types of Land Degradation	Slight Degradation	Medium Degradation	Severe Degradation	Area Proportion of Land Degradation Types
LEV	0.01	0.23	0.32	0.56
LE	0.03	0.02	0.16	0.21
LV	0.04	0.29	0.44	0.77
L	0.11	0.08	0.65	0.84
EV	1	1.27	1.83	4.1
E	3.63	2.26	2.6	8.49
V	20.16	5.49	4.04	29.69
Area proportion of land degradation intensity	24.98	9.64	10.04	\
Types of Land Improvement	Slight Improvement	Apparent Improvement	Proportion of Land Improvement Types	
LEV	0.60	1.19	1.79	
LV	1.26	5.78	7.04	
EV	1.11	6.29	7.40	
V	10.68	28.43	39.11	
Proportion of land improvement	13.65	41.69	\	

Land degradation accounts for 44.66% (Table 5), mainly concentrated in the meadow-dominated areas of the study area. The majority of the study area exhibits slight degradation, covering 24.98% of the total area. An overlap of two or more types of land degradation is observed in 5.64% of the regions, with 4.1% attributed to “EV” degradation, mainly occurring in the central and northeastern parts of the study area (Figure 3a). This finding indicates a certain correlation between grassland degradation and soil erosion. Furthermore, simultaneous “LEV” degradation mainly occurs in the central part of the study area, covering a relatively small area, accounting for only 0.56% of the total area.

3.2. Different Pathways of Land Degradation

3.2.1. Landscape Structure and Quality Degradation

The reduction in grassland patches serves as a key indicator of land degradation. The comparison and analysis of the RFI from 2000 to 2020 reveal that the fragmentation of grassland in the TRHR exhibits significant spatial differentiation (Figure 4). The fragmentation and degradation of grasslands in the TRHR are primarily caused by the expansion of water bodies, the intensification of grassland desertification, and the expansion of cultivated land. In the region shown in Figure 4a, the grassland is encroached upon by sandy land and water bodies, leading to an exacerbation of fragmentation. In the region shown in Figure 4b, grassland fragmentation is also intensifying due to land desertification in specific areas. In the region shown in Figure 4c, abundant water and heat resources increase its suitability for agricultural development, resulting in the encroachment of cultivated land onto some grassland areas. The fragmentation phenomenon has further escalated since 2000, with an intensified total area of $5.05 \times 10^3 \text{ km}^2$. Among these areas, $2.1 \times 10^3 \text{ km}^2$ of grassland patches have disappeared. Conversely, the fragmentation of $6.56 \times 10^3 \text{ km}^2$ of grassland

ecosystem has improved, as indicated by a decreased RFI index of 0.1–0.2. A significant improvement in the RFI index, which decreases by more than 0.2, is observed in an area of $2.5 \times 10^4 \text{ km}^2$. Notably, in the central region of the TRHR, encompassing counties such as Qumalai, Chengduo, Maduo, Xinghai, and others, the improvement in fragmentation is particularly evident.

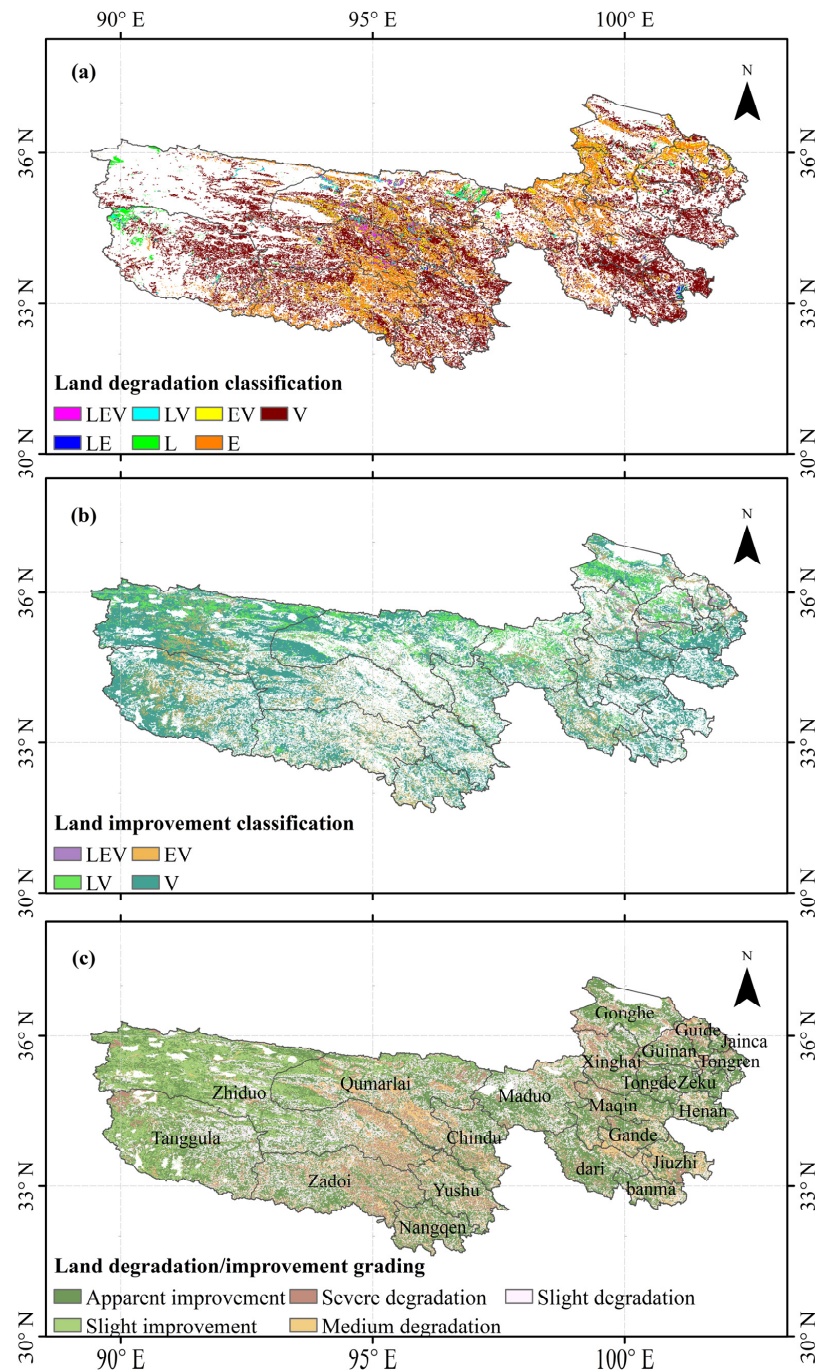


Figure 3. (a) Spatial distribution of types of land degradation in the Three-Rivers Headwater Region; (b) spatial distribution of types of land improvement in the Three-Rivers Headwater Region. (“L”, “E”, and “V” represent landscape, soil erosion, and vegetation, respectively. LEV, LE, LV, and EV represent the overlap of two or three degradation/improvement pathways in the same region); (c) spatial distribution of land degradation/improvement grading in the Three-Rivers Headwater Region.

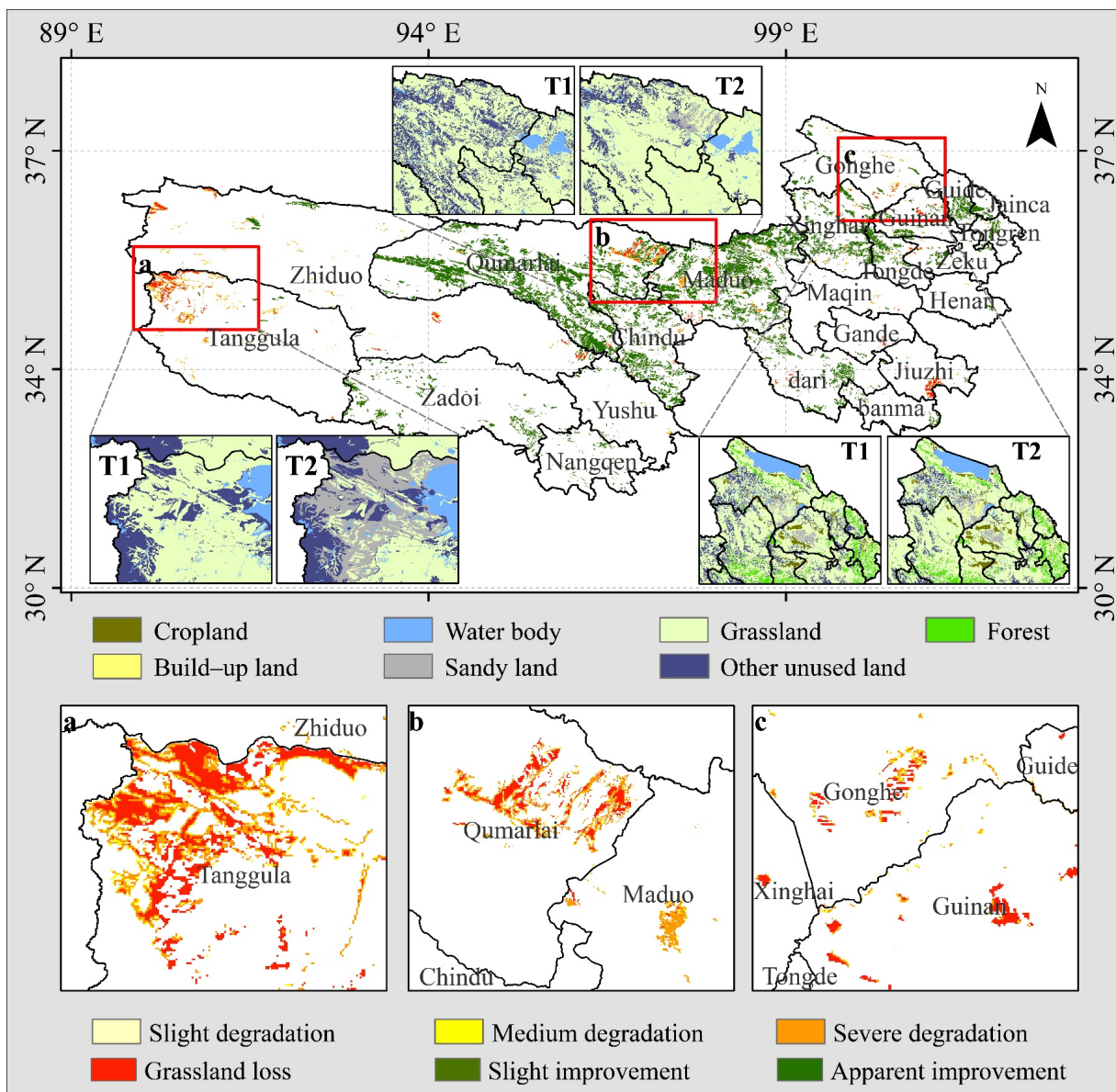


Figure 4. Degree of grassland fragmentation in the Three-Rivers Headwater Region from 2000 to 2020 ((a–c) represent an amplified presentation of grassland fragmentation within three subareas of the research area. T1 and T2 represent land use in 2000 and 2020, respectively).

The habitat quality in the TRHR exhibits a spatial pattern with high and low quality in the east and west, respectively. From 2000 to 2020, the habitat quality remained relatively stable (Figure 5). A slight improvement in habitat quality was observed in the northern part of the TRHR, while a noticeable enhancement in habitat quality was found in the northeastern part of the study area. However, at the junction of Qumalai County and Zhiduo County, the habitat quality experienced a slight decrease, covering an area of $3.06 \times 10^3 \text{ km}^2$. Moderate degradation was mainly observed in the north of Qumalai County, demonstrating a degradation area of only $0.91 \times 10^3 \text{ km}^2$.

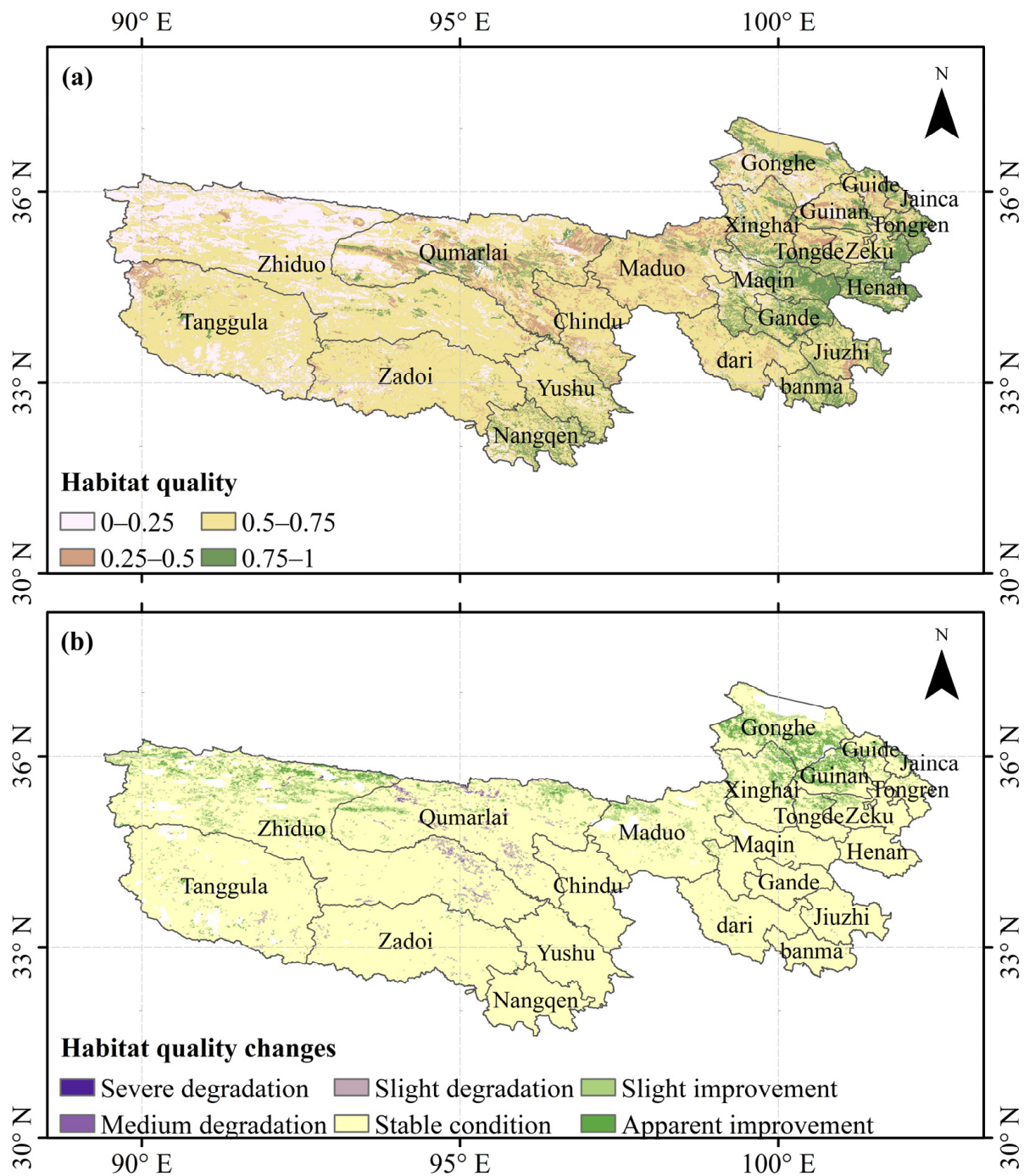


Figure 5. (a) Spatial distribution of the habitat quality in the Three-Rivers Headwater Region; (b) degradation intensity of the habitat quality in the Three-Rivers Headwater Region from 2000 to 2020.

3.2.2. Vegetation Degradation

NDVI exhibits comparable spatial distribution patterns (Figure 6a,b). The median NDVI value for the growing season from May to September was 0.88. In the western region, including Tanggula Mountain Town and Zhiduo County, the NDVI during the vegetation growing season remained relatively low, ranging from 0.1 to 0.2. Overall, the vegetation index in the TRHR displays spatial variation, with values decreasing from southeast to northwest.

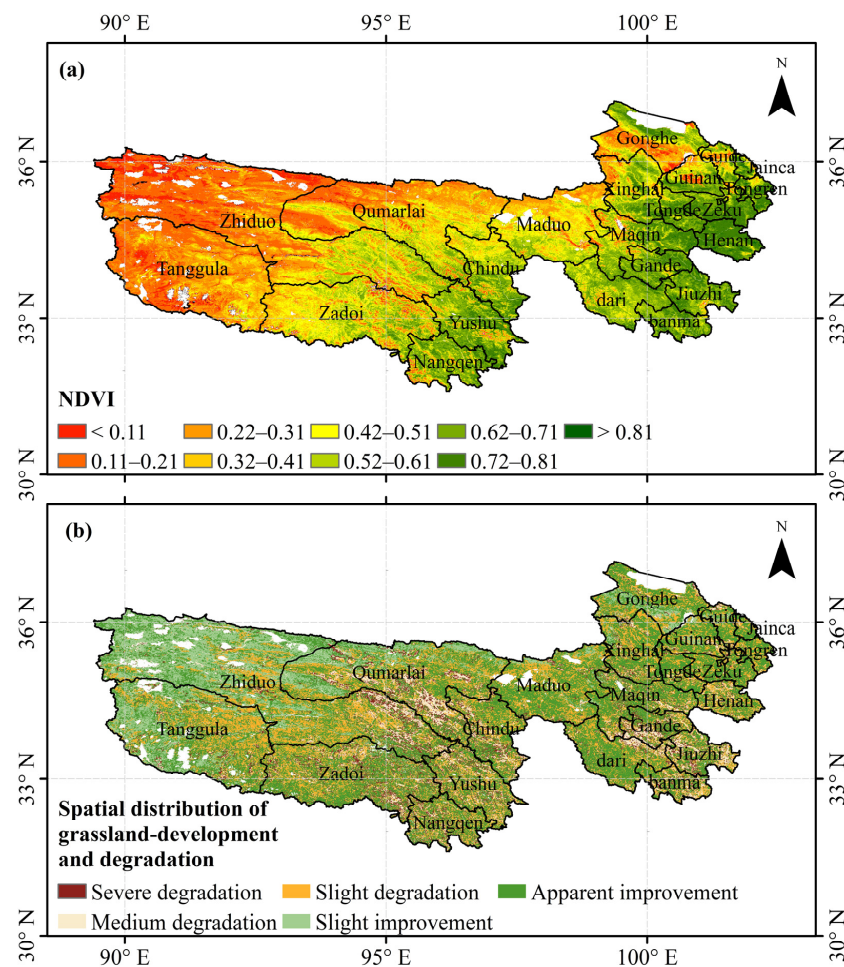


Figure 6. (a) Spatial distribution of the median NDVI value for the growing season from May to September; (b) grassland state improvement (“slight” and “apparent”) and grassland degradation (“slight”, “medium”, and “severe”).

The spatial heterogeneity of grassland cover represented by NDVI in a 1500×1500 m grid was analyzed using a 3×3 pixel moving window. The degradation level in 2020 was classified (Figure 6b) on the basis of the change trend of vegetation indexes. The combination of increased NDVI and increased spatial heterogeneity indicated slight degradation, while that of decreased NDVI and increased spatial heterogeneity indicated medium degradation. The degradation classification framework revealed that 22.26% of the study area was in a state of slight degradation, while 7.21% and 5.63% were in states of medium and severe degradation, respectively (Table 6). These degraded areas were mainly distributed in meadow-dominated regions. Observing the change trend of NDVI, approximately 48.34% of the study areas demonstrated an increasing trend in NDVI and a decreasing trend in spatial heterogeneity, indicating an improvement in the productivity and homogenization of grassland. In sparse vegetation areas with NDVI values less than 0.2, approximately 16.56% of the study areas exhibited signs of grassland regrowth, which was characterized by an increase in NDVI and spatial heterogeneity, particularly in the western part of the study area.

Table 6. Grassland degradation status in the Three-Rivers Headwater Region based on NDVI.

Severe Degradation	Medium Degradation	Slight Degradation	Slight Improvement	Apparent Improvement
5.63%	7.21%	22.26%	16.56%	48.34%

3.2.3. Soil Erosion

The average annual soil erosion amount in the TRHR from 2000 to 2020 was 3.3×10^8 t/a, with a soil erosion modulus of 8.76 t/hm²/a. The TRHR is mainly characterized by its slight and mild erosion, accounting for 90.55% of the total area (Table 7). Areas with a soil erosion intensity greater than 50 t/hm²/a represented 4.34% of the total area and were primarily concentrated in high-altitude regions (Figure 7a).

Table 7. Area percentage of soil erosion intensity classification in different periods and area percentage of soil erosion intensity intensification/amelioration (%).

Classification	Micro	Mild	Moderate	Strong	Extreme	Severe
2000–2010	80.53	9.89	5.22	2.35	1.69	0.32
2011–2020	80.86	9.69	5.03	2.28	1.74	0.40
2000–2020	80.76	9.79	5.11	2.3	1.69	0.35
Degree of soil erosion intensification/amelioration	Apparent improvement	Slight improvement	Stable condition	Slight degradation	Medium degradation	Severe degradation
2000–2020	4.86	8.28	73.50	5.99	3.51	3.86

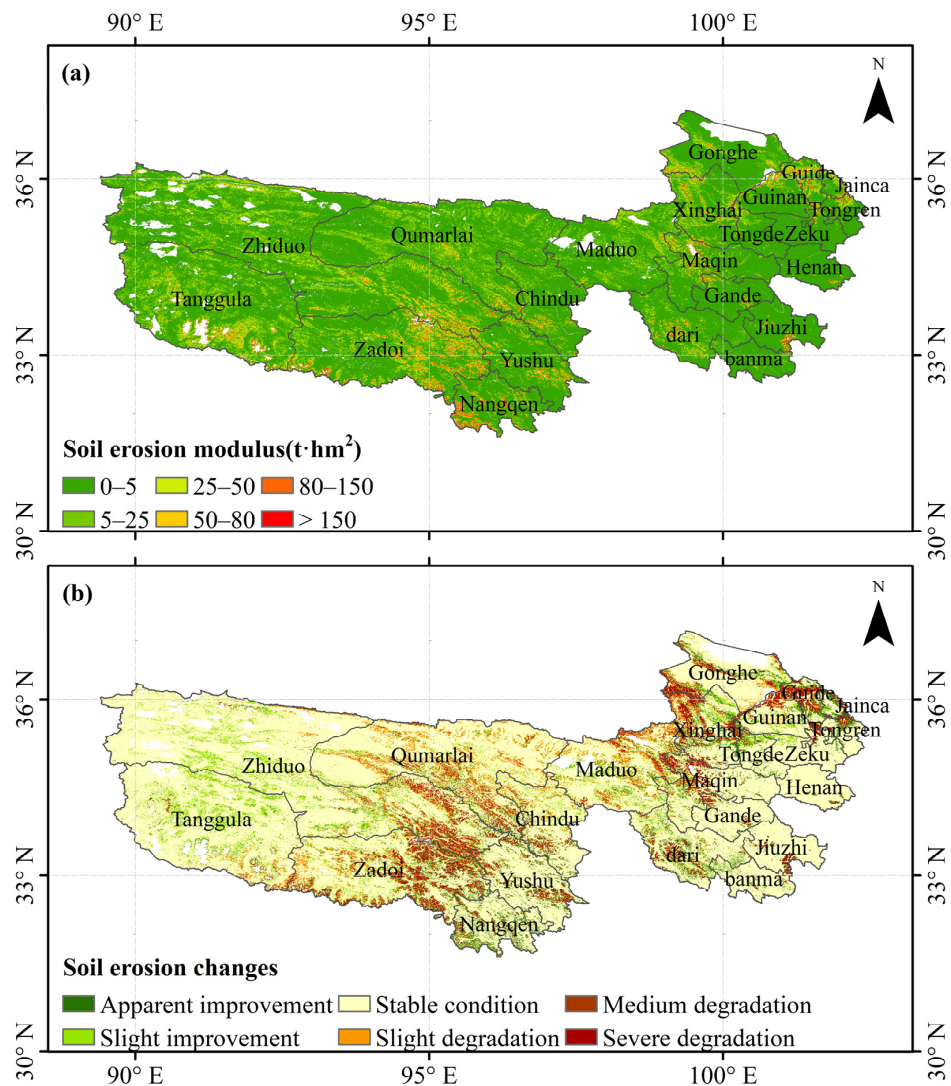


Figure 7. (a) Average soil erosion modulus from 2000 to 2020; (b) degree of soil erosion intensification/amelioration.

The areas of slight, moderate, and severe erosion in the TRHR have all increased from the 2000s to the 2010s. The area of slight erosion has increased by 0.33%, reaching 80.86% (Table 7). However, the proportions of mild, moderate, and severe erosion have decreased, leading to a total reduction in proportion of 0.46%. Over the 20-year period, the average annual soil erosion modulus increased at a rate of 0.03 t/hm²/a. Approximately 73.5% of the TRHR experienced a stable soil erosion modulus during this period (Figure 7b). However, 13.36% of the area showed intensified erosion, with 5.99%, 3.51%, and 3.86% classified as slight, medium, and severe erosion intensification, respectively. The regions with intensified erosion were mainly concentrated in the central and northeastern parts of the study area.

4. Discussion

4.1. Comparison of Land Degradation Assessment Results with Previous Studies

The spatial distribution of fragmentation degradation was obtained by dividing the degree of fragmentation by an interval of 0.1, which demonstrated the stability of the threshold used in this study. The evaluation results of habitat quality were compared with previous studies, and these results revealed that the spatial distribution of habitat quality assessed in this study aligned with that of Hou et al. [44]. Li et al. [21] reported that desertification, severe degradation, medium degradation, and slight degradation occurred in 2%, 8%, 34%, and 21% of the TRHR, respectively, which were generally consistent with the findings. However, the current research indicated that the medium degradation area accounted for 7.21% of the study area, which differed significantly from Li et al. [21]. This discrepancy may be attributed to the extension of the research period to 2020 compared to Li et al., as well as the increase in NDVI, leading to reduced spatial heterogeneity in areas with moderate degradation. By contrast, Wu et al. [46] evaluated the TRHR using the RUSLE model and found that 90.59% and 5.1% of the regions showed slight and severe erosion, respectively. Meanwhile, the increase rate of the soil erosion modulus from 2000 to 2020 was 0.2 t/hm²/a [46], which was consistent with the findings of the current study. Hence, a superposition analysis of land degradation in the TRHR can be further conducted on the basis of the three degradation pathways.

In this study, we also compared our research results with those obtained from other methods applied in the same region. Kang et al. [47] evaluated the land degradation trends in China from 1985 to 2015 based on the NDVI and NPP. The land degradation area in the central part of the TRHR revealed by their study is consistent with the core areas of land degradation D1 (Figure 8) in the current study. Additionally, the northern part of the TRHR is facing challenges from sandstorms and desertification, making it susceptible to erosion [48]. The current study shows that the co-occurrence of soil erosion and grassland degradation is more prevalent in the northern part of the region. Furthermore, a study by Yang et al. [15]—where they utilized NDVI, albedo, and land surface temperature to characterize soil and vegetation degradation in the study area—identified evident land degradation in the north-central and southeast regions of the TRHR, which is largely consistent with the current findings.

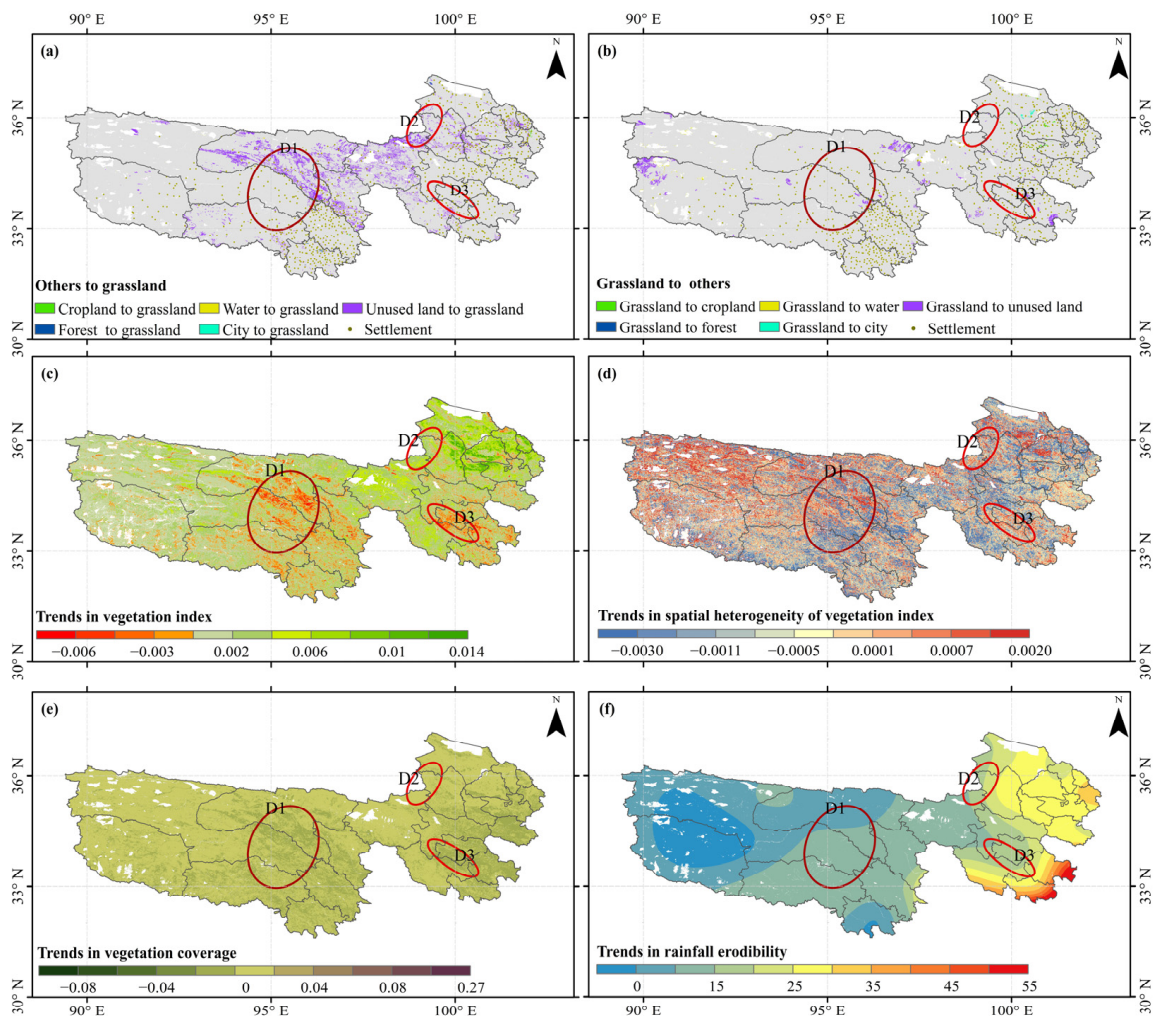


Figure 8. Driving factors of land degradation in the Three-Rivers Headwater Region. (a,b) Transformation of other land types into grassland or grassland into other types. (c) Multi-year variation trend of NDVI. (d) Spatial heterogeneity of NDVI. (e) Vegetation coverage. (f) Rainfall erodibility. D1–D3: core areas of land degradation. (D1–D3 are the core areas of land degradation in the Three-Rivers Headwater Region).

4.2. Driving Forces of Land Degradation

Human activities are the primary driving force behind land degradation in the TRHR. Despite the low population density, the distribution of the population shows distinct spatial variations (Figure 8a,b). The population is concentrated in the central-southern and eastern parts, where water and thermal conditions are highly favorable for agricultural production and grazing. Overgrazing and the increased frequency of fires can exacerbate disturbances, leading to reduced vegetation cover and an elevated risk of soil erosion and desertification [49]. Over the past two decades, approximately 5.24×10^3 km² of grassland has been lost in the TRHR due to desertification and conversion for cultivation purposes. Moreover, the Chinese government has implemented two phases of ecological protection and construction projects in the TRHR since 2000. These projects are aimed at mitigating land degradation and include measures such as restoring degraded grassland (resulting in a 1.98×10^4 km² increase in grassland area between 2000 and 2020), harnessing black soil beaches, and protecting biodiversity. Driven by these projects, the ecological environment in the TRHR has been significantly improved.

Human activities intensify the impact of climate change, exacerbating land degradation. Reductions in vegetation index or vegetation cover have been observed in the core

areas of land degradation D1 and D3, which are areas where two or more types of land degradation occur simultaneously, and the severity of degradation is medium to severe. These reductions in vegetation are concerning because they contribute to an increased risk of soil erosion (Figure 8c,e). The increase in spatial heterogeneity (D2) indicates the fragmentation of vegetation and the development of bare soil patches, which in turn accelerate the expansion of bare land [50] (Figure 8d). Rainfall erodibility has increased in the TRHR in the last 20 years (Figure 8f). Future climate change is expected to exacerbate rainfall erosivity, thus increasing the vulnerability of plateau areas to soil and land degradation. Consequently, these changes will have detrimental effects on the distinctive biodiversity of the region and its ecosystems [11,51]. Furthermore, plateaus face multiple threats, including atmospheric and soil drought, as well as extreme climate events such as exceptionally low or high temperatures. These factors heighten the risk of ecosystem loss and land degradation [52].

4.3. Limitations and Future Work

In addition to the landscape patterns examined in this study, including grassland degradation and soil erosion, other factors contributing to plateau land degradation include wind erosion, freeze–thaw erosion, and desertification. The Tibetan Plateau experiences approximately 150–300 days of temperature fluctuations of approximately 0 °C yearly, leading to frequent freezing and thawing processes [53]. The region above 4500 m above sea level in the TRHR covers 58.46% of the total area and is particularly susceptible to freeze–thaw erosion [54]. Moreover, inadequate precipitation and frequent strong winds increase the susceptibility of the region to desertification [12]. In future studies on land degradation, considering the intensity of freeze–thaw erosion and wind erosion in the study area is crucial.

The TRHR is situated in the transitional zone between seasonally frozen soil and discontinuous and continuous permafrost regions. Based on soil freezing depth observations since the 1960s, a continuous and accelerated decline in freezing depth and duration is observed in the TRHR [55]. Projections indicate that the permafrost area in this region will decrease by 24–28% by 2050 [13]. These changes not only impact the spatial distribution, thermal state, active layer thickness, freeze–thaw state, and snow depth of permafrost but also influence vegetation growth and the capacity of the ecosystem for carbon absorption by altering soil hydrology and nutrients [56]. Moreover, the thawing of permafrost on the plateau will release soil organic carbon into the atmosphere, further contributing to climate warming [57] and adding to the uncertainty of land degradation. In future research, considerable attention should be given to understanding the consequences of permafrost thawing and its effects on land degradation.

5. Conclusions

This study followed the calculation framework of SDG 15.3.1 and utilized various indexes, such as the fragmentation and habitat quality indexes based on land use change, as well as the grassland degradation and water erosion indexes, to assess three distinct pathways of land degradation. These pathways include the degradation of landscape structure and quality, vegetation degradation, and soil erosion. The study determined the extent of land degradation or improvement over time by analyzing the trends of these indicators. Furthermore, the study provided a quantitative analysis of the spatial patterns of land degradation in the TRHR by considering and integrating the three degradation pathways. The main findings of this study are as follows:

- (1) The TRHR exhibits the superimposition of different land degradation pathways. Approximately 5.64% of the regions experience the simultaneous presence of two or more land degradation pathways. However, the superposition of all three degradation paths is observed in only 0.56% of the areas. Notably, the most frequent superposition is between soil erosion and grassland degradation, which accounts for 4.1% of the total area. These findings emphasize the complex nature of land degradation in the

- region and highlight the need for holistic management approaches to address the multiple drivers and impacts of degradation;
- (2) Land degradation in the TRHR is primarily concentrated in the meadow areas. From the perspective of landscape degradation, approximately 2.39% of the study areas exhibit signs of degradation. Based on the classification framework of vegetation degradation, 22.26% of the study areas experienced slight degradation, while 7.21% and 5.63% showed medium and severe degradation, respectively. The soil erosion modulus increased at an average annual rate of 0.03 t/hm²/a over the 20-year period, with 5.99%, 3.51%, and 3.86% of the total area experiencing slight, medium, and severe soil erosion intensification, respectively. These areas are mainly concentrated in the central and northeastern parts of the study area. Implementing robust ecological protection projects in future work is crucial to preventing further land degradation in the TRHR;
 - (3) During the period from 2000 to 2020, the most significant trend observed in the TRHR was land improvement, accounting for 55.34% of the entire region. These land improvement areas were primarily distributed in the western and eastern parts of the region. The regrowth of grassland in the western areas and the improvement and homogenization of grassland productivity in the eastern areas played crucial roles in promoting land improvement.

Author Contributions: Conceptualization, data curation, formal analysis, methodology, writing—original draft, Y.P.; conceptualization, funding acquisition, supervision, writing—review and editing, Y.Y.; review and editing, W.C. All authors have read and agreed to the published version of the manuscript.

Funding: This research was funded by the Second Tibetan Plateau Scientific Expedition Program (2019QZKK0403).

Data Availability Statement: The data presented in this study are available upon request from the corresponding author.

Conflicts of Interest: The authors declare no conflict of interest.

References

1. Právělie, R. Exploring the multiple land degradation pathways across the planet. *Earth-Sci. Rev.* **2021**, *220*, 103689. [[CrossRef](#)]
2. Barbier, E.B.; Hochard, J.P. Land degradation and poverty. *Nat. Sustain.* **2018**, *1*, 623–631. [[CrossRef](#)]
3. Gibbs, H.; Salmon, J.M. Mapping the world's degraded lands. *Appl. Geogr.* **2015**, *57*, 12–21. [[CrossRef](#)]
4. Schillaci, C.; Jones, A.; Vieira, D.; Munafò, M.; Montanarella, L. Evaluation of the United Nations Sustainable Development Goal 15.3.1 indicator of land degradation in the European Union. *Land Degrad. Dev.* **2023**, *34*, 250–268. [[CrossRef](#)]
5. Jiang, L.; Bao, A.; Jiapaer, G.; Liu, R.; Yuan, Y.; Yu, T. Monitoring land degradation and assessing its drivers to support sustainable development goal 15.3 in Central Asia. *Sci. Total Environ.* **2022**, *807*, 150868. [[CrossRef](#)]
6. Yao, T.; Xue, Y.; Chen, D.; Chen, F.; Thompson, L.; Cui, P.; Koike, T.; Lau, W.K.M.; Lettenmaier, D.; Mosbrugger, V.; et al. Recent Third Pole's Rapid Warming Accompanies Cryospheric Melt and Water Cycle Intensification and Interactions between Monsoon and Environment: Multidisciplinary Approach with Observations, Modeling, and Analysis. *Bull. Am. Meteorol. Soc.* **2019**, *100*, 423–444. [[CrossRef](#)]
7. Li, R.; Zhang, M.; Konstantinov, P.; Pei, W.; Tregubov, O.; Li, G. Permafrost degradation induced thaw settlement susceptibility research and potential risk analysis in the Qinghai-Tibet Plateau. *Catena* **2022**, *214*, 106239. [[CrossRef](#)]
8. Wang, X.; Li, X.; Cai, D.; Lou, J.; Li, D.; Liu, F. Salinification and salt transports under aeolian processes in potential desertification regions of China. *Sci. Total Environ.* **2021**, *782*, 146832. [[CrossRef](#)]
9. Yao, T.; Bolch, T.; Chen, D.; Gao, J.; Immerzeel, W.; Piao, S.; Su, F.; Thompson, L.; Wada, Y.; Wang, L.; et al. The imbalance of the Asian water tower. *Nat. Rev. Earth Environ.* **2022**, *3*, 618–632. [[CrossRef](#)]
10. Li, L.; Zhang, Y.; Wu, J.; Li, S.; Zhang, B.; Zu, J.; Zhang, H.; Ding, M.; Paudel, B. Increasing sensitivity of alpine grasslands to climate variability along an elevational gradient on the Qinghai-Tibet Plateau. *Sci. Total Environ.* **2019**, *678*, 21–29. [[CrossRef](#)]
11. Teng, H.; Liang, Z.; Chen, S.; Liu, Y.; Rossel, R.A.V.; Chappell, A.; Yu, W.; Shi, Z. Current and future assessments of soil erosion by water on the Tibetan Plateau based on RUSLE and CMIP5 climate models. *Sci. Total Environ.* **2018**, *635*, 673–686. [[CrossRef](#)] [[PubMed](#)]
12. Teng, Y.; Zhan, J.; Liu, W.; Sun, Y.; Agyemang, F.B.; Liang, L.; Li, Z. Spatiotemporal dynamics and drivers of wind erosion on the Qinghai-Tibet Plateau, China. *Ecol. Indic.* **2021**, *123*, 107340. [[CrossRef](#)]

13. Zhang, G.; Nan, Z.; Hu, N.; Yin, Z.; Zhao, L.; Cheng, G.; Mu, C. Qinghai-Tibet Plateau Permafrost at Risk in the Late 21st Century. *Earth's Future* **2022**, *10*, e2022EF002652. [[CrossRef](#)]
14. Liu, J.; Xu, X.; Shao, Q. Grassland degradation in the “three-river headwaters” region, Qinghai province. *J. Geogr. Sci.* **2008**, *18*, 259–273. [[CrossRef](#)]
15. Yang, L.; Zhao, G.; Mu, X.; Lan, Z.; Jiao, J.; An, S.; Wu, Y.; Miping, P. Integrated assessments of land degradation on the Qinghai-Tibet plateau. *Ecol. Indic.* **2023**, *147*, 109945. [[CrossRef](#)]
16. Sun, Y.; Liu, S.; Shi, F.; An, Y.; Li, M.; Liu, Y. Spatio-temporal variations and coupling of human activity intensity and ecosystem services based on the four-quadrant model on the Qinghai-Tibet Plateau. *Sci. Total Environ.* **2020**, *743*, 140721.
17. Kumar, B.P.; Babu, K.R.; Anusha, B.; Rajasekhar, M. Geo-environmental monitoring and assessment of land degradation and desertification in the semi-arid regions using Landsat 8 OLI/TIRS, LST, and NDVI approach. *Environ. Chall.* **2022**, *8*, 100578. [[CrossRef](#)]
18. Sun, X.; Li, S.; Zhai, X.; Wei, X.; Yan, C. Ecosystem changes revealed by land cover in the three-river headwaters region of Qinghai, China (1990–2015). *Res. Cold Arid Reg.* **2023**, *15*, 85–91. [[CrossRef](#)]
19. Mao, D.; Wang, Z.; Wu, B.; Zeng, Y.; Luo, L.; Zhang, B. Land degradation and restoration in the arid and semiarid zones of China: Quantified evidence and implications from satellites. *Land Degrad. Dev.* **2018**, *29*, 3841–3851. [[CrossRef](#)]
20. Zhang, S.; Wu, T.; Guo, L.; Zou, H.; Shi, Y. Integrating ecosystem services supply and demand on the Qinghai-Tibetan Plateau using scarcity value assessment. *Ecol. Indic.* **2023**, *147*, 109969. [[CrossRef](#)]
21. Li, C.; de Jong, R.; Schmid, B.; Wulf, H.; Schaepman, M.E. Changes in grassland cover and in its spatial heterogeneity indicate degradation on the Qinghai-Tibetan Plateau. *Ecol. Indic.* **2020**, *119*, 106641. [[CrossRef](#)]
22. Li, X.L.; Perry, G.; Brierley, G.; Sun, H.Q.; Li, C.H.; Lu, G.X. Quantitative assessment of degradation classifications for degraded alpine meadows (heitutan), Sanjiangyuan, western China. *Land Degrad. Dev.* **2014**, *25*, 417–427. [[CrossRef](#)]
23. Giuliani, G.; Mazzetti, P.; Santoro, M.; Nativi, S.; Van Bemmelen, J.; Colangeli, G.; Lehmann, A. Knowledge generation using satellite earth observations to support sustainable development goals (SDG): A use case on Land degradation. *Int. J. Appl. Earth Obs. Geoinf.* **2020**, *88*, 102068. [[CrossRef](#)]
24. Assennato, F.; Di Leginio, M.; d’Antona, M.; Marinosci, I.; Congedo, L.; Riitano, N.; Luise, A.; Munafò, M. Land degradation assessment for sustainable soil management. *Ital. J. Agron.* **2020**, *15*, 299–305. [[CrossRef](#)]
25. Zheng, L.; Wang, Y.; Li, J. Quantifying the spatial impact of landscape fragmentation on habitat quality: A multi-temporal dimensional comparison between the Yangtze River Economic Belt and Yellow River Basin of China. *Land Use Policy* **2023**, *125*, 106463. [[CrossRef](#)]
26. Xoxo, S.; Mantel, S.; De Vos, A.; Mahlaba, B.; Le Maitre, D.; Tanner, J. Towards SDG 15.3: The biome context as the appropriate degradation monitoring dimension. *Environ. Sci. Policy* **2022**, *136*, 400–412. [[CrossRef](#)]
27. Easdale, M.H.; Fariña, C.; Hara, S.; León, N.P.; Umaña, F.; Tittone, P.; Bruzzone, O. Trend-cycles of vegetation dynamics as a tool for land degradation assessment and monitoring. *Ecol. Indic.* **2019**, *107*, 105545. [[CrossRef](#)]
28. Morales, N.S.; Zuleta, G.A. Comparison of different land degradation indicators: Do the world regions really matter? *Land Degrad. Dev.* **2020**, *31*, 721–733. [[CrossRef](#)]
29. Tsymbarovich, P.; Kust, G.; Kumani, M.; Golosov, V.; Andreeva, O. Soil erosion: An important indicator for the assessment of land degradation neutrality in Russia. *Int. Soil Water Conserv. Res.* **2020**, *8*, 418–429. [[CrossRef](#)]
30. Zhao, L.; Yu, W.; Meng, P.; Zhang, J.; Zhang, J. InVEST model analysis of the impacts of land use change on landscape pattern and habitat quality in the Xiaolangdi Reservoir area of the Yellow River basin, China. *Land Degrad. Dev.* **2022**, *33*, 2870–2884. [[CrossRef](#)]
31. Maurya, S.; Srivastava, P.K.; Gupta, M.; Islam, T.; Han, D. Integrating soil hydraulic parameter and microwave precipitation with morphometric analysis for watershed prioritization. *Water Resour. Manag.* **2016**, *30*, 5385–5405. [[CrossRef](#)]
32. Li, W.; Wang, D.; Li, Y.; Zhu, Y.; Wang, J.; Ma, J. A multi-faceted, location-specific assessment of land degradation threats to peri-urban agriculture at a traditional grain base in northeastern China. *J. Environ. Manag.* **2020**, *271*, 111000. [[CrossRef](#)] [[PubMed](#)]
33. Zhang, H.; Jiang, C.; Wang, Y.; Wang, J.; Li, C.; Yang, Z.; Gong, Q.; Yang, C. Improving the integrated efficacy of ecosystem restoration efforts by linking land degradation neutrality to ecosystem service enhancement from a spatial association perspective. *Ecol. Eng.* **2022**, *181*, 106693. [[CrossRef](#)]
34. Zhang, L.; Zhang, H.; Xu, E. Information entropy and elasticity analysis of the land use structure change influencing eco-environmental quality in Qinghai-Tibet Plateau from 1990 to 2015. *Environ. Sci. Pollut. Res.* **2022**, *29*, 18348–18364. [[CrossRef](#)]
35. Zhao, D.; Zhu, Y.; Wu, S.; Lu, Q. Simulated response of soil organic carbon density to climate change in the Northern Tibet permafrost region. *Geoderma* **2022**, *405*, 115455. [[CrossRef](#)]
36. Liu, S.; Shao, Q.; Ning, J.; Niu, L.; Zhang, X.; Liu, G.; Huang, H. Remote-sensing-based assessment of the ecological restoration degree and restoration potential of ecosystems in the upper yellow river over the past 20 years. *Remote Sens.* **2022**, *14*, 3550. [[CrossRef](#)]
37. Rivas, C.A.; Guerrero-Casado, J.; Navarro-Cerillo, R.M. Deforestation and fragmentation trends of seasonal dry tropical forest in Ecuador: Impact on conservation. *For. Ecosyst.* **2021**, *8*, 46. [[CrossRef](#)]
38. Fischer, R.; Taubert, F.; Müller, M.S.; Groeneveld, J.; Lehmann, S.; Wiegand, T.; Huth, A. Accelerated forest fragmentation leads to critical increase in tropical forest edge area. *Sci. Adv.* **2021**, *7*, eabg7012. [[CrossRef](#)]

39. Zhu, C.; Zhang, X.; Zhou, M.; He, S.; Gan, M.; Yang, L.; Wang, K. Impacts of urbanization and landscape pattern on habitat quality using OLS and GWR models in Hangzhou, China. *Ecol. Indic.* **2020**, *117*, 106654. [[CrossRef](#)]
40. Huang, Z.; Bai, Y.; Alatalo, J.M.; Yang, Z. Mapping biodiversity conservation priorities for protected areas: A case study in Xishuangbanna Tropical Area, China. *Biol. Conserv.* **2020**, *249*, 108741. [[CrossRef](#)]
41. Terrado, M.; Sabater, S.; Chaplin-Kramer, B.; Mandle, L.; Ziv, G.; Acuna, V. Model development for the assessment of terrestrial and aquatic habitat quality in conservation planning. *Sci. Total Environ.* **2016**, *540*, 63–70. [[CrossRef](#)] [[PubMed](#)]
42. Polasky, S.; Nelson, E.; Pennington, D.; Johnson, K.A. The Impact of Land-Use Change on Ecosystem Services, Biodiversity and Returns to Landowners: A Case Study in the State of Minnesota. *Environ. Resour. Econ.* **2011**, *48*, 219–242. [[CrossRef](#)]
43. Rimal, B.; Sharma, R.; Kunwar, R.; Keshtkar, H.; Stork, N.E.; Rijal, S.; Rahman, S.A.; Baral, H. Effects of land use and land cover change on ecosystem services in the Koshi River Basin, Eastern Nepal. *Ecosyst. Serv.* **2019**, *38*, 100963. [[CrossRef](#)]
44. Hou, Y.; Zhao, W.; Liu, Y.; Yang, S.; Hu, X.; Cherubini, F. Relationships of multiple landscape services and their influencing factors on the Qinghai-Tibet Plateau. *Landsc. Ecol.* **2021**, *36*, 1987–2005. [[CrossRef](#)]
45. Williams, J.R. The erosion-productivity impact calculator (EPIC) model: A case history. *Philos. Trans. R. Soc. London Ser. B Biol. Sci.* **1990**, *329*, 421–428.
46. Wu, D.; Peng, R.; Huang, L.; Cao, W.; Huhe, T. Spatio-Temporal Analysis and Driving Factors of Soil Water Erosion in the Three-River Headwaters Region, China. *Water* **2022**, *14*, 4127. [[CrossRef](#)]
47. Kang, J.; Zhang, Y.; Biswas, A. Land degradation and development processes and their response to climate change and human activity in China from 1982 to 2015. *Remote Sens.* **2021**, *13*, 3516. [[CrossRef](#)]
48. Zhang, C.; Li, Q.; Shen, Y.; Zhou, N.; Wang, X.; Li, J.; Jia, W. Monitoring of aeolian desertification on the Qinghai-Tibet Plateau from the 1970s to 2015 using Landsat images. *Sci. Total Environ.* **2018**, *619*, 1648–1659. [[CrossRef](#)]
49. Bardgett, R.D.; Bullock, J.M.; Lavorel, S.; Manning, P.; Schaffner, U.; Ostle, N.; Chomel, M.; Durigan, G.; Fry, E.L.; Johnson, D.; et al. Combatting global grassland degradation. *Nat. Rev. Earth Environ.* **2021**, *2*, 720–735. [[CrossRef](#)]
50. Tang, Z.; Zhang, Y.; Cong, N.; Wimberly, M.; Wang, L.; Huang, K.; Li, J.; Zu, J.; Zhu, Y.; Chen, N. Spatial pattern of pika holes and their effects on vegetation coverage on the Tibetan Plateau: An analysis using unmanned aerial vehicle imagery. *Ecol. Indic.* **2019**, *107*, 105551. [[CrossRef](#)]
51. Jiang, C.; Zhang, L. Climate Change and Its Impact on the Eco-Environment of the Three-Rivers Headwater Region on the Tibetan Plateau, China. *Int. J. Environ. Res. Public Health* **2015**, *12*, 12057–12081. [[CrossRef](#)] [[PubMed](#)]
52. Zhang, Y.; Hong, S.; Liu, D.; Piao, S. Susceptibility of vegetation low-growth to climate extremes on Tibetan Plateau. *Agric. For. Meteorol.* **2023**, *331*, 109323. [[CrossRef](#)]
53. Xie, S.; Qu, J.; Xu, X.; Pang, Y. Interactions between freeze–thaw actions, wind erosion desertification, and permafrost in the Qinghai–Tibet Plateau. *Nat. Hazards* **2017**, *85*, 829–850. [[CrossRef](#)]
54. Wang, X.; Zhao, X.; Zhang, Z.; Yi, L.; Zuo, L.; Wen, Q.; Liu, F.; Xu, J.; Hu, S.; Liu, B. Assessment of soil erosion change and its relationships with land use/cover change in China from the end of the 1980s to 2010. *Catena* **2016**, *137*, 256–268. [[CrossRef](#)]
55. Luo, S.; Fang, X.; Lyu, S.; Jiang, Q.; Wang, J. Interdecadal changes in the freeze depth and period of frozen soil on the Three Rivers Source Region in China from 1960 to 2014. *Adv. Meteorol.* **2017**, *2017*, 5931467. [[CrossRef](#)]
56. Lv, M.; Wang, Y.; Gao, Z. The change process of soil hydrological properties in the permafrost active layer of the Qinghai–Tibet Plateau. *CATENA* **2022**, *210*, 105938. [[CrossRef](#)]
57. Wang, T.; Zhao, Y.; Xu, C.; Ciais, P.; Liu, D.; Yang, H.; Piao, S.; Yao, T. Atmospheric dynamic constraints on Tibetan Plateau freshwater under Paris climate targets. *Nat. Clim. Chang.* **2021**, *11*, 219–225. [[CrossRef](#)]

Disclaimer/Publisher’s Note: The statements, opinions and data contained in all publications are solely those of the individual author(s) and contributor(s) and not of MDPI and/or the editor(s). MDPI and/or the editor(s) disclaim responsibility for any injury to people or property resulting from any ideas, methods, instructions or products referred to in the content.